THE JOURNAL OF BIOLOGICAL CHEMISTRY VOL. 289, NO. 12, pp. 8375–8389, March 21, 2014

Rab10-mediated Endocytosis of the Hyaluronan Synthase HAS3 Regulates Hyaluronan Synthesis and Cell Adhesion to Collagen*

Received for publication, January 21, 2014 Published, JBC Papers in Press, February 7, 2014, DOI 10.1074/jbc.M114.552133

Ashik Jawahar Deen[‡1], Kirsi Rilla[‡2], Sanna Oikari[‡§2], Riikka Kärnä[‡], Genevieve Bart[‡], Jukka Häyrinen[‡], Avinash Rahul Bathina[‡], Antti Ropponen[¶], Katri Makkonen[‡], Raija H. Tammi[‡], and Markku I. Tammi[‡3]

From the Institutes of [‡]Biomedicine, [§]Clinical Medicine and [¶]Dentistry, School of Medicine, University of Eastern Finland, Kuopio 70210, Finland

Background: Hyaluronan synthases (HASs) require transport to plasma membrane for the activation of hyaluronan (HA) synthesis.
Results: Rab10 overexpression inhibited, whereas Rab10 silencing increased, cell surface HA coat and HAS3-dependent hyaluronan synthesis.
Conclusion: Rab10 reduces the steady-state abundance of HAS3 in the plasma membrane by enhancing HAS3 endocytosis.
Significance: HA synthesis is controlled by HAS3 endocytosis mediated by Rab10.

Hyaluronan synthases (HAS1–3) are unique in that they are active only when located in the plasma membrane, where they extrude the growing hyaluronan (HA) directly into cell surface and extracellular space. Therefore, traffic of HAS to/from the plasma membrane is crucial for the synthesis of HA. In this study, we have identified Rab10 GTPase as the first protein known to be involved in the control of this traffic. Rab10 colocalized with HAS3 in intracellular vesicular structures and was co-immunoprecipitated with HAS3 from isolated endosomal vesicles. Rab10 silencing increased the plasma membrane residence of HAS3, resulting in a significant increase of HA secretion and an enlarged cell surface HA coat, whereas Rab10 overexpression suppressed HA synthesis. Rab10 silencing blocked the retrograde traffic of HAS3 from the plasma membrane to early endosomes. The cell surface HA coat impaired cell adhesion to type I collagen, as indicated by recovery of adhesion following hyaluronidase treatment. The data indicate a novel function for Rab10 in reducing cell surface HAS3, suppressing HA synthesis, and facilitating cell adhesion to type I collagen. These are processes important in tissue injury, inflammation, and malignant growth.

Hyaluronan (HA)[4] is a ubiquitous non-sulfated extracellular glycosaminoglycan consisting of repeating disaccharide units of -(β1–4-glucuronic acid-β1–3-*N*-acetyl glucosamine)-. It is produced by many animal cell types (1) and is involved in a number of cell signaling systems (2), contributing to processes like cell migration, differentiation, and proliferation (3). HA plays crucial roles in inflammation and several of its pathological manifestations like cancer, diabetes, and arterial diseases through its interaction and signaling with various cell surface receptors (*i.e.* CD44, RHAMM, TLR2/4, etc.) (2, 4).

HA, unlike all other vertebrate sugar polymers, is synthesized directly into the extracellular space by a family of transmembrane glycosyltransferases called hyaluronan synthases (HAS1–3) (5). When overexpressed, HAS3 induces the formation of microvillus-like plasma membrane protrusions in several cell types (6), and the synthesis of HA takes place on these HAS3-induced protrusions. When HAS3 is unable to reach the plasma membrane, the synthesis of HA is impaired (7). Although a fair amount of information is available on HAS gene expression (8), data on the post-translational modifications of HASs (*i.e.* phosphorylation (9), ubiquitination (10), and *O*-GlcNAcylation (11)) have emerged only recently, and nothing is known about the machinery controlling their traffic to plasma membrane (8). The intracellular traffic of HASs is another facet of post-translational processes, which can significantly affect the enzymatic activity of HASs and thereby control HA synthesis.

To explore the mechanisms involved in the trafficking of HAS, we subjected cytoplasmic vesicles immunoprecipitated with a GFP-HAS3 antibody to mass spectrometric screening for associated proteins. Several proteins belonging to the vesicular trafficking machinery were identified, including Rab10, a member of the Rab family, comprising more than 60 proteins. They are master regulators of several aspects of intracellular traffic like transporting cargos from the *trans*-Golgi network to the

* This work was supported by the Academy of Finland (to M. I. T.), the Sigrid Juselius Foundation (to M. T. and R. T.), Kuopio University Hospital (to E. V. O. and M. I. T.), and Spearhead Funds from the University of Eastern Finland (Cancer Center of Eastern Finland) (to M. I. T. and R. T.).
[1] Supported by grants from the Finnish Glycoscience Graduate School, CIMO Foundation, and Finnish Cultural Foundation.
[2] Both authors contributed equally to this work.
[3] To whom correspondence should be addressed: Institute of Biomedicine, School of Medicine, University of Eastern Finland, Yliopistonranta 1E, P.O. Box 1627, 70211, Kuopio, Finland. Tel.: 358-40-7674826; Fax: 358-17-163032; E-mail: tammi@uef.fi.
[4] The abbreviations used are: HA, hyaluronan; HAS, hyaluronan synthase; HABC, hyaluronan-binding complex; fHABC, fluorescent HABC; ER, endoplasmic reticulum; EEA1, early endosome antigen 1; ROI, region of interest; PB, 0.1 M sodium phosphate buffer, pH 7.0; PFA, paraformaldehyde; PNS, postnuclear supernatant; MDCK, Madin-Darby canine kidney; EGFP, enhanced green fluorescent protein; PFA, paraformaldehyde; ANOVA, analysis of variance.

plasma membrane (12, 13). Because Rab10 GTPase was one of the most prominent proteins found in our screen for HAS3-associated proteins, we focused on it in this work. It turned out that Rab10 was indeed functionally important in the traffic of HAS3 but, unexpectedly, promoted depletion of HAS3 from plasma membrane. This enhancement of reverse traffic or endocytosis of a specific cargo is a completely novel function for Rab10. We show that Rab10 is a suppressor of HA synthesis and suggest that trafficking of HAS to/from plasma membrane forms a more important regulatory step in HA synthesis than previously anticipated.

EXPERIMENTAL PROCEDURES

Cell Culture—Canine kidney epithelial cell line (MDCK) stably overexpressing EGFP-HAS3 (14) was cultured in Dulbecco's minimal essential medium (Euroclone, Pero (Milan), Italy) with 10% fetal bovine serum (Hyclone, Logan, UT), 4 mM glutamine (Sigma), 50 μg/ml streptomycin sulfate, and 50 units/ml penicillin (Sigma). MCF7, a breast adenocarcinoma cell line, was cultured in minimal essential medium α (Euroclone) with 5% fetal bovine serum (Hyclone), 4 mM glutamine (Sigma), 50 μg/ml streptomycin sulfate, and 50 units/ml penicillin (Sigma).

MCF7 Cells Stably Expressing EGFP-HAS3—The generation of MCF7 cells stably overexpressing doxycycline-inducible EGFP-HAS3 was described before (15). Cells with optimal EGFP-HAS3 expression following 1 μg/ml doxycycline induction were sorted by a flow cytometer and maintained in growth media with 50 μg/ml hygromycin. The reproducibility and consistency of the EGFP-HAS3 expression in response to doxycycline (Sigma) were determined with HA assays.

Plasmids and Antibodies—Construction of EGFP-HAS3 (14) and Dendra2-HAS3 (16) plasmids, expressing human HAS3, has been described previously. HAS3-Myc, expressing human HAS3 (gift from Dr. Sakari Kellokumpu, University of Oulu, Finland), EGFP-Rab10 (gift from Dr. Kenneth W. Dunn, Indiana University), and Rpre-mRFP (Addgene plasmid 17275, deposited by Dr. Sergio Grinstein (17)) were used. mRFP-HAS3 and 6Myc-HAS3 were made by subcloning HAS3 cDNA in mRFP-C1 and 6Myc-pcDNA3 vectors, respectively. For FRET analysis, mCherry fluorescent tag was added to HAS3 in the N and C terminus as follows. mCherry-HAS3 was made by replacing EGFP in the EGFP-HAS3 construct (14), using NheI and XhoI restriction sites. HAS3-mCherry was made by inserting HAS3 into the vector pcDNA-Cerulean, described before (18), and then replacing mCerulean by mCherry using XhoI and NotI restriction sites.

Rabbit polyclonal anti-calnexin (Cell Signaling, Danvers, MA), rabbit polyclonal anti-pan-cadherin (Abcam, Cambridge, UK), rabbit polyclonal anti-Golgin 97 (Abcam), rabbit polyclonal anti-clathrin heavy chain (Cell signaling), mouse monoclonal 9E10 anti-c-Myc antibody (Santa Cruz Biotechnology, Inc.), rabbit polyclonal anti-GFP (Invitrogen), rabbit monoclonal anti-Rab5 and anti-Rab7 (Cell Signaling), rabbit polyclonal anti-EEA1 (Cell Signaling), goat polyclonal anti-rabbit and anti-mouse Dylight 680 (Thermo Scientific), and Texas Red-labeled anti-mouse and anti-rabbit antibodies (Vector Laboratories) were also used.

Subcellular Fractionation—MCF7 cells were grown in 10-cm dishes and co-transfected with HAS3-Myc and EGFP-Rab10 using ExGen 500 transfection reagent (Fermentas, Thermo Scientific) according to the manufacturer's instructions. All of the steps during cell lysis and fractionation were done at 4 °C, unless stated otherwise. Nearly confluent cells were washed twice and scraped off in phosphate-buffered saline (PBS). The cells were pelleted down at 200 $\times$ *g* and resuspended in cold lysis buffer with no detergent (25 mM Tris, 150 mM NaCl, and 1 mM $CaCl_2$, pH 7.8, with complete protease inhibitor mixture (Sigma)) and sonicated (Heilscher Ultrasonics, D-70184, Stuttgart, Germany). The resulting cell lysate was centrifuged at 200 $\times$ *g* for 5 min, 1000 $\times$ *g* for 10 min, and 6400 $\times$ *g* for 15 min to remove intact cells, nuclei, and mitochondria, respectively. Part of the postnuclear supernatant (PNS) was mixed with 62% sucrose solution to make 40.6% PNS sucrose mix. In the ultracentrifuge tube, a gradient of 50% sucrose, 40.6% PNS mix, 35% sucrose, and 25% sucrose solutions and lysis buffer was prepared and then centrifuged in a Sorvall ultracentrifuge with a TH641 rotor at 154,000 $\times$ *g* for 18 h. 22 fractions were collected, beginning from the topmost layer of the gradient (*labeled 1–22* in Fig. 1). The fractions were tested for specific organelle markers (calnexin (endoplasmic reticulum), Rab5 and Rab7 (endosomes), pan-cadherin (plasma membrane), and Golgin 97 (Golgi)) in Western blots.

Co-immunoprecipitation—Fractions corresponding to endosomes, plasma membrane, and Golgi were pooled together, and 100–500 μg of protein samples, estimated by BCA assay (Pierce, Thermo Scientific), were taken from each pool for co-immunoprecipitation. The fractions were precleared overnight with normal mouse IgG conjugated with protein A/G magnetic beads (Ademtech, 33600 Pessac, France). The precleared samples were incubated overnight with c-Myc antibody and immunoprecipitated with protein A/G magnetic beads. The beads were washed three times with cold lysis buffer, and proteins were eluted with 0.2 M glycine-HCl, pH 2.5, and diluted with 0.5 M Tris-HCl, 1.5 M NaCl, pH 7.4. The eluted samples were heated with 4$\times$ SDS sample buffer at 65 °C for 15 min and stored at −20 °C. The samples were subjected to immunoblotting with c-Myc and anti-GFP antibodies.

Mass Spectrometry—MDCK cells with stable, high expression of EGFP-HAS3 was chosen for mass spectrometry to ensure a sufficiently high signal (14). About 500 μg of PNS from MDCK-EGFP-HAS3 cells was immunoprecipitated with anti-GFP antibody, as described above. The result of immunoprecipitation was confirmed by Western blot with anti-GFP antibody, and the rest of the sample was subjected to SDS-PAGE. Trypsin digests were prepared using sequencing grade trypsin (Sigma) and extracted, and the mass spectra were analyzed using an LC-electrospray ionization-MS/MS system, as described previously (19). For MS/MS ion search (20), automated spectral processing, peak list generation, and database search from raw data were performed on a separate work station using Analyst QS version 1.1 and the MASCOT search version 1.6b13 script for Analyst QS (Applied Biosystems). The MASCOT search algorithm was used via Mascot-script online (21), and a SwissProt database search (version 2010_12) was utilized. Other parameters set for the MS/MS ion search were

TABLE 1
PCR and siRNA sequences

Gene	Sequence
Rab10 PCR primers	5′-GTGGGGAAGACCTGCGTCCTTT-3′ 5′-GGAGGTTGTGATGGTGTGAAATCGC-3′
Rab35 PCR primers	5′-CGGTGTGGGCAAGAGCAGTTTAC-3′ 5′-TGACAAAGGACTCGGCACTGGT-3′
GAPDH PCR primers	5′-AGAAGGCTGGGGCTCATTTG-3′ 5′-AGGGGCCATCCACAGTCTTC-3′
Rab10 siRNA	Sense: GCUGAAGAUAUCCUUCGAA Antisense: UUCGAAGGAUAUCUUCAGC
Negative control siRNA (scrambled)	Eurogentec (Reference no.: SR-CL000-005)

the same as discussed previously (19). Protein hits were selected based on the p value ($p < 0.05$) for extensive homology, calculated by the MASCOT algorithm. The identified protein hits were screened according to the Mascot score of the matched peptides, and the sequence coverage of the proteins was calculated.

Western Blotting—Protein fractions from sucrose gradient centrifugation or co-immunoprecipitation were subjected to 10% SDS-PAGE, and the proteins were transferred to nitrocellulose membranes (Protran, Whatman), blocked with 3 or 5% bovine serum albumin (BSA) in 1× TBST (Tris-buffered saline containing 0.1% Tween 20) for 1 h at room temperature, followed by overnight incubation with the primary antibodies, anti-GFP (1:1000), anti-calnexin (1:1000), anti-pan-cadherin (1:500), anti-Golgin 97 (1:1000) and anti-c-Myc antibody (1:500) diluted in 1% BSA-TBST, anti-Rab5 (1:1000) diluted in TBST, and anti-Rab7 (1:1000) diluted in 5% BSA-TBST. After three washes with TBST, the membranes were incubated for 1 h at room temperature with the infrared secondary antibodies, anti-rabbit or anti-mouse Dylight 680 (1:5000) and anti-goat Alexa Fluor 680 (1:5000), diluted in 1% BSA-TBST, and washed three times with TBST. The protein bands in the blots were visualized on a LI-COR Odyssey Infrared imaging system (LI-COR Biosciences, Lincoln, NE).

siRNA Silencing of Rab10—The Rab10 and scrambled siRNAs were obtained from Eurogentec (Seraing, Belgium), with the sequences given in Table 1. About 250,000 MCF7 cells were seeded on 6-well plates and grown until 50% confluence, treated with 30 nM siRNA using Lipofectamine RNAiMax reagent (Invitrogen), according to the manufacturer's instructions. 48 h later, the cells were lysed; total RNA was isolated using Tri Reagent (Molecular Research Center Inc., Cincinnati, OH); and the cDNAs were synthesized using the Verso cDNA kit (Thermo Scientific). The quantitative real-time PCR was performed with Fast Start Universal SYBR Green mix (Roche Applied Science) using the Stratagene Mx3000P real-time PCR system (Agilent Technologies). Relative mRNA expression levels were compared by using the $2^{-\Delta\Delta C(T)}$ method, with GAPDH as a control. The primer sequences used for real-time PCR are given in Table 1.

The protein expression of Rab10 after siRNA silencing was quantified by transient transfection of 0.75 μg/well of EGFP-Rab10. The cells were harvested and lysed, and PNS was obtained as described above. The amount of protein in all of the lysate samples was quantified by a BCA assay. 100 μl of cell lysate/well was added in a 96-well plate, and the GFP fluorescence was measured in a microplate reader equipped with a 355-nm UV lamp and 485/535-nm (excitation/emission) filters. The samples were also subjected to Western blotting with anti-GFP antibody.

Hyaluronan Secretion—2×10^5 MCF7-EGFP-HAS3 cells were plated on 6-well plates, as duplicates, and treated with siRNAs, as described above. 24 h after siRNA transfection, the growth medium was replaced with one containing 0.25 μg/ml doxycycline to induce the expression of EGFP-HAS3. After 24 h, the media from the treated groups were collected and stored at −20 °C for later assays of HA, and the cell numbers were counted to express the HA content as ng/10,000 cells. The amount of HA secreted into growth medium was determined by an enzyme-linked sorbent assay, as described before (22).

Confocal Microscopy and Live Cell Imaging—The fluorescent images were obtained with ×40 numerical aperture 1.3 and ×63 numerical aperture 1.4 oil objectives (512 × 512-pixel resolution) on a Zeiss Axio Observer inverted microscope equipped with a Zeiss LSM 700 confocal module (Carl Zeiss Microimaging). For live cell imaging, a Zeiss XL-LSM S1 incubator with temperature and CO_2 control was used. DRAQ5 nuclear staining (2 μM, Biostatus Ltd., Leicestershire, UK) was used to evaluate the transfection efficiency and to count the total number of cells in a field.

Immunofluorescence—The MCF7 cells were co-transfected with 6Myc-HAS3 and EGFP-Rab10 or EGFP (mock transfection) using ExGen 500 (Invitrogen) according to the manufacturer's instructions. The same method was followed for mRFP-HAS3. 24 h after transfection, the cells were fixed with 4% paraformaldehyde (PFA) in 0.1 M sodium phosphate buffer (PB), pH 7.4, for 1 h and washed five times with PB. The fixed cells were permeabilized for 10 min with 0.1% Triton X-100 in 1% BSA, blocked with 1% BSA for 20 min, and incubated overnight with anti-c-Myc primary antibody (1:100) in 1% BSA at 4 °C. After washing, the cells were incubated with Texas Red-labeled secondary anti-mouse antibody (1:500 in PB) for 1 h and washed with PB. The cells were then incubated with DRAQ5 for 5 min, washed with PB, and stored at 4 °C.

Clathrin Heavy Chain Staining—MCF7 cells were transfected with EGFP-HAS3 or EGFP (mock) and fixed with 4% PFA, and the cells were stained with anti-clathrin heavy chain antibody (1:100 in 1% BSA-PB) and Texas Red-labeled anti-rabbit antibody (1:500 in PB). The stained cells were then imaged with a ×40 oil objective for colocalization analysis.

Colocalization Analysis—For colocalization analysis, images were taken with a ×63 or ×40 oil objective, and the analysis was done with BioImageXD software (23), unless otherwise specified. The autothreshold function was used to process and analyze the colocalized pixels. Pearson's correlation coefficient (*Rr*) was used to measure the degree of colocalization, with 10–15 images/group. The colocalized images are shown as 8-bit or 1-bit representations.

FRET Assay by Acceptor Photobleaching—MCF7 cells were transfected with a combination of plasmids as follows: EGFP-Rab10 and HAS3 with the N-terminal mCherry, EGFP-Rab10 and the HAS3 with the C-terminal mCherry, and EGFP (mock) and mCherry-HAS3. 24 h later, the cells were fixed with 4% PFA and mounted with an antifade reagent, Mowiol® 4-88 (Sigma).

To measure FRET efficiency, regions Of interest (ROIs) were randomly positioned inside the cells and also outside the cells for background subtraction. mCherry was photobleached using a 555-nm laser at 100% strength, with 25 iterations, and then second pictures of both fluorophores were taken. Images were analyzed using Fiji (24). FRET efficiency (E) was calculated for each pixel in the bleached area using the equation, $E\% = (I^{\text{Donor postbleach}} - I^{\text{Donor prebleach}})/I^{\text{Donor postbleach}} \times 100$, where I^{Donor} represents the intensity of EGFP fluorescence. For each ROI, FRET efficiency was calculated from the average fluorescence intensities of the donor before and after bleaching the acceptor and corrected with the change in EGFP fluorescence intensity outside the bleached area. Means and S.E. of the efficiencies were calculated for each combination of the fluorophores.

Image Processing—Microscopic images were processed with ZEN 2009 software (Carl Zeiss Microimaging GmbH). In some experiments, cell numbers were counted using the ImageJ program (Fiji, available on the World Wide Web). For image presentation, Adobe Photoshop Elements version 9 software (Adobe Systems) was used. Images were brightness/contrast-adjusted, and in some cases non-linear adjustment was used uniformly across the control and treated groups to better show the cellular features of interest.

Hyaluronan Coat Analysis—For visualization of HA surface coat on live cells, HA-binding complex (HABC) conjugated to Alexa Fluor 568 or AlexaFluor 647 was used as described previously (25). The cells were imaged with a ×40 oil objective from 15 random fields. For quantitative analysis, the cells were also imaged with a ×20 objective from 15 random fields in each group with 1500–2200 cells, using z-stacks of 1.93-μm thickness. The mean intensity of HA coat (Alexa Fluor 568, red) from the images was quantified from the compressed z-stacks of 320 × 320-μm area, divided by the total number of positive cells, visualized by DRAQ5 nuclear staining.

Analysis of Plasma Membrane Residence of HAS3—siRNA-treated MCF7 cells were transiently transfected with EGFP-HAS3 and Rpre-mRFP in a 3:1 ratio. 24 h later, the cells were fixed with 4% PFA. Individual cells from each treatment were imaged with the same acquisition settings, using a ×40 oil objective. The images were processed and analyzed with the ZEN 2009 software. ROIs were drawn around plasma membrane, marked with Rpre-mRFP, and the whole cell, and the integrated intensity in each of the ROIs was calculated. The plasma membrane residence index of EGFP-HAS3 was calculated as the ratio of integrated intensity in plasma membrane to the whole cell and expressed as a percentage.

Analysis of HAS3 Retrograde Traffic—siRNA-treated MCF7 cells were transfected with Dendra2-HAS3. 24 h later, HA coat was stained with 2 μg/ml Alexa Fluor 647-labeled HABC (fHABC) for 0.5 h at 37 °C. The ROI was marked around the cell surface with HA coat as a reference, and Dendra2-HAS3 was photoconverted with 15% of the 405-nm laser power, 10 iterations, for 1 s. The time point after photoconversion was set as "0", and time lapse images were taken for 16 min with 2-min intervals. The retrograde traffic of Dendra2-HAS3 away from the cell surface was analyzed with fHABC as the reference signal, and the results were expressed as -fold changes of Dendra2-HAS3/fHABC ratio from time point 0.

HAS3 Endocytosis—siRNA-treated MCF7 cells were transfected with EGFP-HAS3 or mRFP-HAS3 and, 24 h later, treated with markers for clathrin-dependent and fluid phase endocytosis. For clathrin-dependent endocytosis, the cells were incubated with transferrin conjugated to fluorescein (Invitrogen), and the transferrin uptake assay was done as described previously (26, 27). The cells were fixed with 4% PFA, washed with PB, and stored at 4 °C before microscopy. For fluid phase endocytosis, the cells were incubated with growth medium containing 0.5 mM Alexa Fluor®-hydrazide 594 (Invitrogen) for 2 h at 37 °C. The cells were then washed with PB; fixed with 4% PFA, 2% glutaraldehyde; washed with PB; and stored at 4 °C. Images were taken as z-stack sections at 0.39-μm intervals with a ×63 oil objective. Colocalization between HAS3 and the endocytosis markers was analyzed.

HAS3 Colocalization with EEA1—siRNA-treated MCF7 cells were transfected with EGFP-HAS3. 24 h later, the cells were fixed with 4% PFA, incubated with EEA1 antibody (1:100, 1% BSA-PB), and stained with Texas Red-labeled anti-rabbit antibody (1:500 in PB), as described before. At least 15 images were taken from each group with a ×63 oil objective. Three ROIs were drawn randomly outside of the nucleus and perinuclear Golgi region in the images, and the average colocalization, with the threshold set to 50 arbitrary units, was calculated from the ROIs using ZEN 2009 software.

Cell Proliferation Assay—130,000 cells/well of MCF7-EGFP-HAS3 or MCF7 cells were seeded in 12-well plates as duplicates, after siRNA transfection, as described above. 24 h later, new medium with or without 0.25 μg/ml doxycycline was changed to MCF7-EGFP-HAS3 and MCF7 cells, respectively. The cell numbers were counted after 24, 48, and 72 h, and the result was expressed as cells/0.5 ml.

Cell Adhesion Assay with 3-(4,5-Dimethylthiazol-2-yl)-2,5-diphenyltetrazolium Bromide Colorimetric Method—MCF7-EGFP-HAS3 or parental MCF7 cells were transfected with Rab10 siRNA and control siRNA, and the former was induced with 0.25 μg/ml doxycycline for the expression of EGFP-HAS3. The cells were also treated with hyaluronidase (5 turbidity reducing units/ml in PBS) (Seikagaku Biobusiness, Chiyoda-ku, Tokyo, Japan) or PBS alone, in growth media, for 6 h before starting the adhesion experiment. A 96-well plate was precoated overnight with 0.25 mg/ml collagen type I (BD Biosciences) and 1% BSA-PBS (negative control) and blocked with 0.1% BSA-PBS for 1 h at 37 °C prior to the experiment. The cells were trypsinized, neutralized with trypsin-neutralizing solution (ScienCell, Carlsbad, CA), and centrifuged at 1000 × g for 5 min. The cell pellet was resuspended in DMEM (no phenol red; Euroclone) with 0.1 mg/ml cycloheximide (Sigma) and counted. 20,000 cells (adjusted to 100 μl/well) were added in six independent wells for each group. In some experiments, external high molecular mass HA (Healon, Abbott) at 50, 200, and 500 μg/ml concentrations was included. The cells were incubated at 37 °C for 30 min in DMEM without phenol red and then gently washed away with PBS. 100 μl/well DMEM (no phenol red) diluted 1:10 with 3-(4,5-dimethylthiazol-2-yl)-2,5-diphenyltetrazolium bromide (Sigma; 5 mg/ml in PBS) was

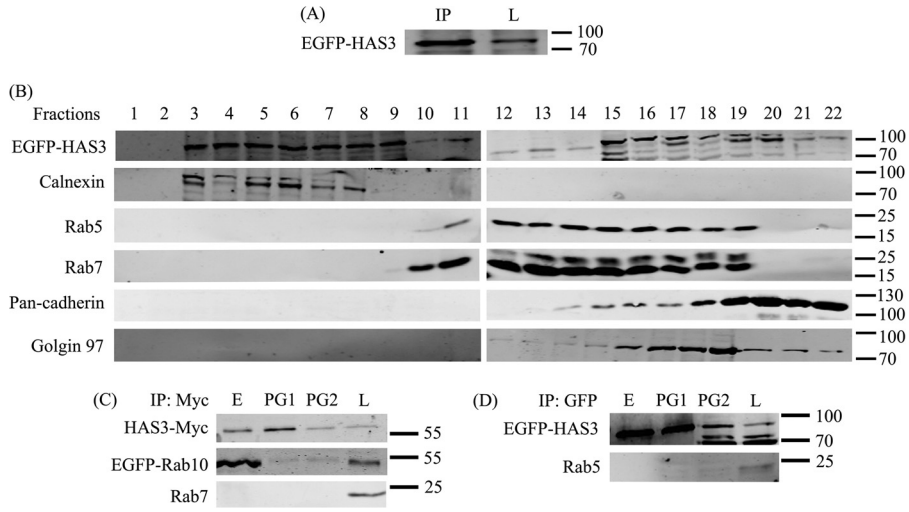

FIGURE 1. **Co-immunoprecipitation of HAS3 and Rab10.** *A*, EGFP-HAS3 was immunoprecipitated from total cell lysate of MDCK cells and identified by anti-GFP antibody in Western blot. *IP*, immunoprecipitate; *L*, total cell lysate. *B*, the distribution of EGFP-HAS3 (~90 kDa) in the sucrose gradient fractions was analyzed with anti-GFP antibody, and different subcellular organelles in the fractions were identified using the markers calnexin (ER) in fractions 3–8, Rab5 and Rab7 (endosomes) in fractions 10–14, and pan-cadherin (plasma membrane) and Golgin 97 (Golgi) in fractions 15–22. Fractions 10–14 were pooled for endosomes, thus excluding those (15–19) positive also for the indicators of Golgi and plasma membrane. *C*, HAS3-Myc and EGFP-Rab10 were co-transfected in MCF7 cells. Myc antibody immunoprecipitated EGFP-Rab10 and HAS3-Myc from endosomes, whereas another common endosomal protein (Rab7) did not co-immunoprecipitate with HAS3-Myc. *D*, EGFP-HAS3 was transiently transfected in MCF7 cells, immunoprecipitated with anti-GFP antibody, and analyzed for the presence of Rab5, another common endosomal protein. Rab5 did not co-immunoprecipitate with EGFP-HAS3. *E*, endosomes; *PG1* and *PG2*, plasma membrane + Golgi mix, in fractions 10–14 and 15–22, respectively. *L*, total cell lysate. In some parts of the gradient, the anti-GFP antibody produced several apparently nonspecific bands in addition to that of GFP-HAS3 at ~90 kDa.

TABLE 2
Proteins detected in EGFP-HAS3 immunoprecipitate by LC-MS/MS

Identified protein[a]	Accession no.	Sequence coverage	Mascot score[b]
		%	
Rab10-GTPase	P61026	13	45
Sorting nexin 2 (SNX2)	Q9UNH7	3.08	50
Sorting nexin 6 (SNX6)	Q6P8X1	7.88	46
Clathrin heavy chain-1	Q00610	0.65	39
AP-1 complex subunit β-1	Q10567	2.42	51

[a] Significant protein hits ($p < 0.05$) are shown; p value for extensive homology was calculated by Mascot database search. The Uniprot accession number is shown here.
[b] Mascot score >39 indicates identity for the matched peptides.

added to the cells, incubated at 37 °C for 2 h, and carefully removed. The reaction was stopped with 100 μl/well DMSO with gentle shaking for 5 min, and the absorbance was measured at 540 and 620 nm (for background subtraction).

Statistical Analysis—All statistical tests were done in GraphPad Prism version 5.0. One-way ANOVA with Tukey's post hoc test and paired Student's *t* test was used. Observations with a p value of <0.05 were considered to be statistically significant.

RESULTS

Association of HAS3 with Rab10 in Transport Vesicles—Because nothing was known about the vehicles transporting the HAS proteins between the Golgi complex and plasma membrane, we started by isolating the endosomal vesicles of cells expressing EGFP-HAS3 or HAS3-Myc. Immunoprecipitation of EGFP-HAS3 from the total cell lysate of MDCK-EGFP-HAS3 cells (Fig. 1*A*), followed by mass spectrometric analysis of the proteins brought down with the EGFP antibody, revealed several components associated with endosomal traffic, as listed in Table 2. We focused on Rab10, one of the significant hits, because it has been shown to be important for the traffic from *trans*-Golgi to the plasma membrane. Western blotting of subcellular fractions indicated the presence of EGFP-HAS3 in the endoplasmic reticulum (ER; indicated by calnexin), plasma membrane (pan-cadherin positivity), and Golgi complex (identified by Golgin 97), as expected, and also in endosomal vesicles (identified by Rab5 and Rab7 positivity) (Fig. 1*B*). We then co-transfected EGFP-Rab10 and HAS3-Myc in MCF7 cells and immunoprecipitated HAS3-Myc from different subcellular organelle fractions. Western blot analysis of the immunoprecipitated cellular organelles showed that HAS3 co-immunoprecipitated with Rab10, mainly in the endosomes (Fig. 1*C*). In contrast, two other trafficking-related proteins, Rab7 and Rab5, were not co-immunoprecipitated with HAS3 (Fig. 1, *C* and *D*). This suggests that HAS3 was specifically associated with those endosomal vesicles that contain Rab10.

Colocalization analysis was used to gain more support for the presence of HAS3 and Rab10 in the same transport vesicles. Two different tags for HAS3 (*i.e.* mRFP and 6Myc) were used in these experiments to rule out tag-dependent, possibly nonspecific interactions with EGFP-Rab10. HAS3 indeed colocalized in cytoplasmic vesicles with EGFP-Rab10 (Fig. 2*A*). Mock transfection (EGFP vector), used as a negative control, did not show colocalization. Colocalization analysis using Pearson's correlation coefficient showed that both mRFP-HAS3 and 6Myc-HAS3 strongly colocalized with Rab10 ($Rr = 0.53$ and 0.47, respectively) when compared with EGFP mock transfection ($Rr = 0.13$ and 0.08, respectively) (Fig. 2*B*).

We then studied the proximity of HAS3 and Rab10 in the endosomes using FRET (Förster resonance energy transfer) analysis. We studied the FRET efficiency between EGFP-Rab10 and mCherry positioned in the N or C terminus of HAS3, co-transfected in MCF7 cells. The minor FRET efficiencies

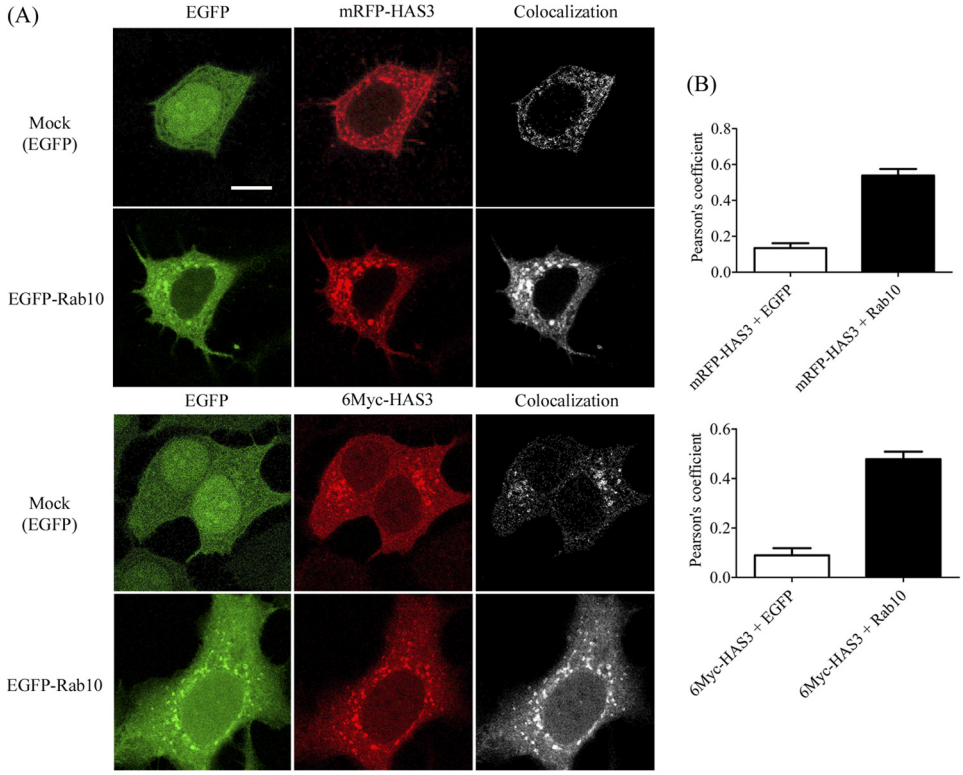

FIGURE 2. **Colocalization of HAS3 and Rab10.** *A*, EGFP-Rab10 was colocalized with mRFP-HAS3 and 6Myc-HAS3 in cytoplasmic vesicles. EGFP (mock transfection) showed very little colocalization with mRFP-HAS3. *Scale bar*, 10 μm. *B*, quantitative colocalization assays of mRFP-HAS3 and 6Myc-HAS3 with EGFP-Rab10 showed higher values for Pearson's correlation coefficient when compared with the EGFP (mock) group (mean ± S.E. (*error bars*) of three independent experiments, each with 15 images/group).

between EGFP-Rab10 and N- and C-terminally mCherry-tagged HAS3, 3.6 ± 0.6% (n = 8) and 3.1 ± 0.6% (n = 13), respectively, suggest that HAS3 and Rab10 were not within a 10-nm distance of each other. We thus conclude that although HAS3 resides in Rab10-positive vesicles, there is probably no direct interaction between the two proteins.

Silencing of Rab10 by siRNA—Having confirmed the presence of HAS3 in the Rab10-positive vesicles, it was essential to study its functional significance in HAS3 traffic. To be used as a standard model for this study, we have made MCF7 cells with stable, inducible expression of EGFP-HAS3, called MCF7-EGFP-HAS3 cells (Fig. 3*A*). The doxycycline-treated cells showed HAS3-dependent, microvillus-like plasma membrane protrusions coated with HA (Fig. 4*E*) and also a dose-dependent increase of HA secretion in the medium (Fig. 3*B*). We utilized siRNA against Rab10 to silence its expression. The Rab10 mRNA levels were reduced to 30 ± 5% of control (mean ± S.E.) in 48 h, whereas the mRNA level of Rab35, another factor involved in endosomal traffic, was not affected (94 ± 5% of control), suggesting specificity of the siRNA. Because we could not find a good working antibody for Rab10, transfection of EGFP-Rab10 was utilized to test the silencing in protein level. By measuring the GFP fluorescence/mg of total protein, we found that the expression of EGFP-Rab10 following Rab10-siRNA treatment was reduced to 29 ± 18% of non-treated cells as compared with 99 ± 7% following control siRNA. A similar result was observed in Western blot analysis (Fig. 3*C*). In contrast, no alteration was found in Rab7 (Fig. 3*C*). Therefore, the siRNA-mediated knockdown of Rab10 was

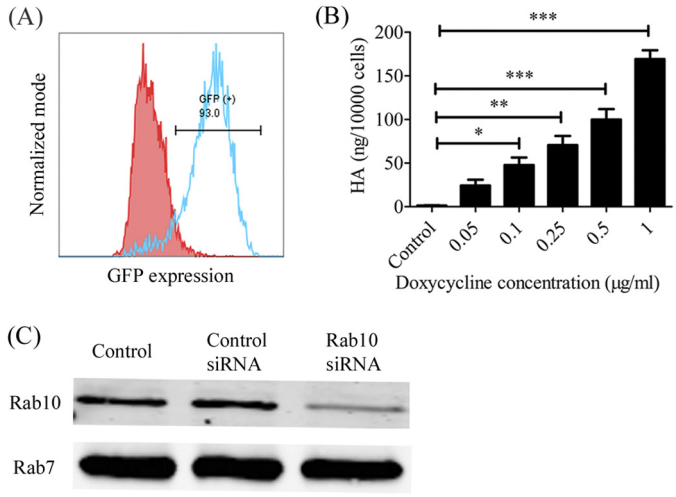

FIGURE 3. **Stable transfection of EGFP-HAS3 and silencing Rab10 expression in MCF7 cells.** *A*, MCF7 cells were transduced with lentiviral vectors carrying doxycycline-inducible EGFP-HAS3 and hygromycin resistance genes and maintained in selective growth media with 0.25 mg/ml hygromycin. The expression of EGFP-HAS3 was induced with 1 μg/ml doxycycline, and the cells with high EGFP expression were selected using FACS as indicated with the *bar*. *B*, the selected MCF7-EGFP-HAS3 cells with doxycycline-inducible EGFP-HAS3 expression showed a dose-dependent increase of HA secreted in the medium after 48 h. Data represent mean ± S.E. (*error bars*) of three independent experiments. *, $p < 0.05$; **, $p < 0.01$; ***, $p < 0.001$ (one-way ANOVA, Tukey's test). *C*, EGFP-Rab10 was transiently expressed in the cells treated with Rab10 siRNA, along with the controls, and the cell lysate was analyzed by Western blots with an anti-GFP antibody. The expression of Rab10 was markedly reduced, whereas Rab7 was not altered.

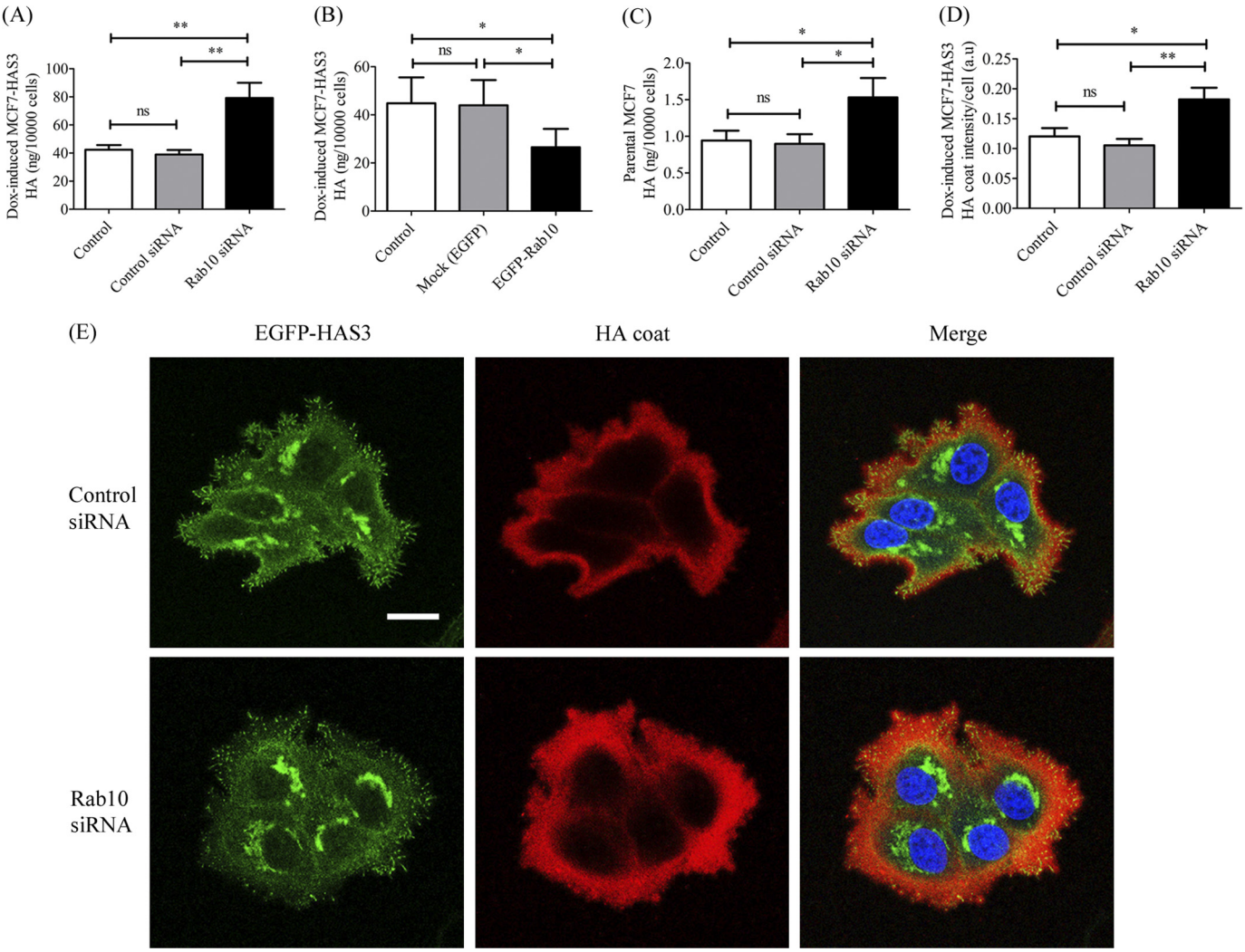

FIGURE 4. **HA secretion and surface coat formation is influenced by Rab10.** *A*, control and Rab10 siRNA-treated MCF7-EGFP-HAS3 cells were induced with 0.25 μg/ml doxycycline for 24 h for EGFP-HAS3 expression, and the media were assayed for HA synthesis. Rab10 silencing significantly increased HA synthesis. *B*, MCF7-EGFP-HAS3 cells were transfected with EGFP-Rab10 and EGFP only (mock), and induced with 0.25 μg/ml doxycycline for 24 h, and the media were analyzed for HA. HA secretion was significantly decreased when EGFP-Rab10 was overexpressed. *C*, parental MCF7 cells without HAS3 overexpression were treated with Rab10 siRNA along with the control groups, and the media were collected 48 h later. Rab10 silencing increased HA secretion compared with the control groups. Data in *A–C* represent mean ± S.E. (*error bars*) of 5 independent experiments. *, $p < 0.05$; **, $p < 0.01$; *ns*, not significant (paired *t* test). *D*, HA surface coat formation was analyzed in MCF7-EGFP-HAS3 cells with 0.5 μg/ml doxycycline induction. Quantitative image analysis was done with a ×20 objective. A significant increase in HA surface coat was observed with Rab10 silencing, compared with the control and control siRNA groups. Data represent mean ± S.E. of three independent experiments from >1500 cells/group in 15 random fields. *, $p < 0.05$; **, $p < 0.01$; *ns*, not significant (one-way ANOVA, Tukey's test). *E*, representative images taken with a ×40 objective show the increased HA coat by Rab10 silencing. Nuclei (*blue*) were stained with DRAQ5. *Scale bar*, 20 μm.

effective and specific enough to study its impact on HAS3 traffic.

Silencing of Rab10 did not change the general pattern of GFP-HAS3 distribution in MCF7 cells (Fig. 4*E*). Changes in the general morphology of ER were not observed either, using the distribution of calnexin as a marker.

Rab10 Expression Influences HA Secretion into Growth Medium and HAS3-induced HA Surface Coat Formation—Because HA is synthesized only when HAS3 is located in the plasma membrane, an increase or decrease in the amount of HA secreted into growth medium is a good indicator for the change in HAS3 traffic. Rab10 silencing with siRNA induced a 2-fold increase of HA, compared with the control siRNA group (Fig. 4*A*). The opposite effect was obtained by overexpression of EGFP-Rab10, which caused a significant decline in HA secretion (Fig. 4*B*). Rab10 silencing significantly increased HA synthesis also by endogenous HAS in cells without HAS3 transfection (Fig. 4*C*). These results indicated that the association between Rab10 and HAS3 has functional consequences (*i.e.* Rab10 suppresses HA secretion).

During HA synthesis, the growing polysaccharide chain is bound to HAS3, creating the plasma membrane protrusions typical for this HAS (6) and building a HA coat on the cell surface (8). Because HA secretion was increased with silencing of Rab10, and HA is attached to HAS3 during its synthesis, we anticipated that there is also a significant change in the size of pericellular HA coat in MCF7-EGFP-HAS3 cells. As expected, Rab10 silencing significantly increased the size of the pericellular HA coat compared with the control and control siRNA groups. Quantitative analysis with a total of 1500–2000 cells/

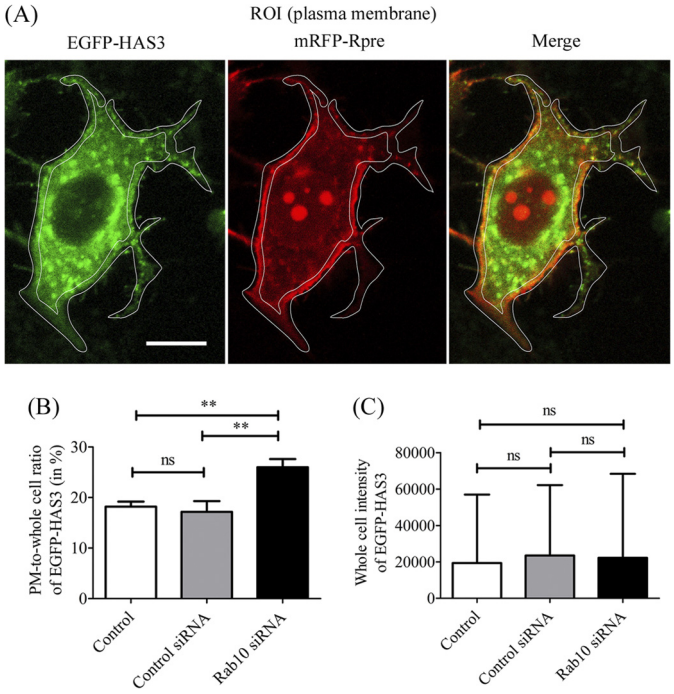

FIGURE 5. **Plasma membrane residence of HAS3 is increased by Rab10 silencing.** *A*, a ROI (*white line*) was set around the plasma membrane marked with mRFP-Rpre. *Scale bar*, 10 μm. *B*, the plasma membrane/whole cell ratio of EGFP-HAS3 indicated that Rab10 silencing increased the plasma membrane residence of EGFP-HAS3. *C*, the whole cell signal of EGFP-HAS3 was not altered by the treatments. Data represent means ± S.E. (*error bars*) of three independent experiments, each containing 14–15 images/group. **, $p < 0.001$; *ns*, not significant (one-way ANOVA, Tukey's test).

group, taken with a ×20 objective, showed that Rab10 silencing induced a 1.75-fold increase in HA coat size compared with the control siRNA group (Fig. 4*D*). Representative images, taken with a higher magnification, also confirmed the fact that Rab10 silencing increased the size of HA coat when compared with the control siRNA-treated cells (Fig. 4*E*). This, along with the HA assay in medium confirms that Rab10 silencing influences HAS3-dependent HA synthesis.

Silencing of Rab10 Increases HAS3 Residence in Plasma Membrane—Because Rab10 silencing increased HA synthesis, a direct analysis of plasma membrane residence of HAS3 was done in MCF7 cells. Following Rab10 silencing, we transiently co-transfected EGFP-HAS3 and a plasma membrane marker, Rpre-mRFP, which is a K-Ras-derived polypeptide sequence targeted to the inner leaflet of the plasma membrane (17). Using the Rpre-mRFP-positive region as a reference, the plasma membrane signal of EGFP-HAS3 was measured. The integrated intensities were measured from ROIs drawn around the plasma membrane (Fig. 5*A*), and the plasma membrane/whole cell ratio of EGFP-HAS3 fluorescence was calculated. The analysis showed that Rab10 silencing increased the plasma membrane residence of HAS3 by 1.5-fold, compared with the control and control siRNA groups (Fig. 5*B*). There was no significant difference in the overall EGFP signal in the whole cells between the groups (Fig. 5*C*). This observation, along with the previous results, showed that Rab10 silencing increases the plasma membrane residence of HAS3.

Retrograde Traffic of Has3 from Cell Surface Is Decreased with Silencing of Rab10—We then analyzed the rate of retrograde traffic of HAS3 from plasma membrane to the interior of the cell. Following Rab10 silencing, we transiently transfected Dendra2-HAS3 in MCF7 cells. A ROI was drawn on the cell surface using the HA coat, stained with the fHABC as a reference. Using a photoconversion technique in which part of the green Dendra2-HAS3 was turned red, the retrograde traffic of Dendra2-HAS3 from the cell surface was estimated by time lapse imaging of the red signal. In the control and control siRNA groups, HAS3 traffic from the cell surface was so fast that a notable amount of red HAS3 was seen all around the cytoplasm already in 2 min (Fig. 6*A*). In the control and control siRNA groups, the average $t_{1/2}$ of cell surface Dendra2-HAS3 was only 5–6 min (Fig. 6*B*). Rab10 silencing dramatically reduced the retrograde traffic of Dendra2-HAS3 from the cell surface, obviously with a $t_{1/2}$ far beyond the 16-min follow-up (Fig. 6*B*). Quantitative analysis of the kinetics of Dendra2-HAS3 showed that at the end of the 16-min period, Rab10 silencing increased Dendra2-HAS3 residence on the cell surface to 73% of the starting value, compared with 31 and 30% in control and control siRNA groups, respectively (Fig. 6*B*). This result was in line with the observation that Rab10 silencing increases plasma membrane residence of HAS3 and suggested that Rab10 increases endocytosis of HAS3 from the plasma membrane.

Rab10 Regulates Clathrin-dependent Endocytosis of HAS3—HAS3 co-immunoprecipitated with clathrin heavy chain (Table 2), and clathrin heavy chain colocalized with EGFP-HAS3 ($Rr = 0.46$), compared with empty EGFP vector ($Rr = 0.19$) (Fig. 7, *A* and *C*). To learn more about the type of HAS3 endocytosis and thus the target of Rab10, we checked the colocalization of HAS3 with clathrin-mediated and fluid phase endocytosis markers. Transferrin and Alexa Fluor® hydrazide 594 were used as markers to study clathrin-dependent and fluid phase endocytosis, respectively. MCF7 cells transiently transfected either with mRFP-HAS3 or EGFP-HAS3 were then incubated with fluorescein-labeled transferrin or Alexa Fluor® hydrazide 594 and fixed. Colocalization analysis showed that HAS3 partially colocalized with transferrin ($Rr = 0.24$) but not with Alexa Fluor® hydrazide 594 ($Rr = 0.07$) (Fig. 7, *B* and *D*). These data suggest that HAS3 mainly follows clathrin-dependent endocytosis.

The effect of Rab10 on the clathrin-dependent endocytosis of HAS3 was studied by measuring the colocalization of HAS3 and transferrin. Following Rab10 silencing, we transiently transfected the cells with mRFP-HAS3, incubated them with fluorescein-labeled transferrin, and fixed them. Images were taken as *z*-stacks with an optical section thickness of 0.39 μm, spanning the whole cell. The results showed that HAS3 colocalization with transferrin was reduced in cells subjected to Rab10 silencing (Fig. 8*A*), and the quantitative analysis showed that Pearson's coefficient in the Rab10 silencing group was significantly reduced ($Rr = 0.13$), compared with control and control siRNA groups ($Rr = 0.24$ and 0.21, respectively) (Fig. 8*B*). Transferrin uptake in the cells was not affected by the siRNA treatments, as judged by the mean fluorescent intensity of transferrin (Fig. 8*C*). This shows that Rab10 silencing specifically decreased endocytosis of HAS3, which also substantiates

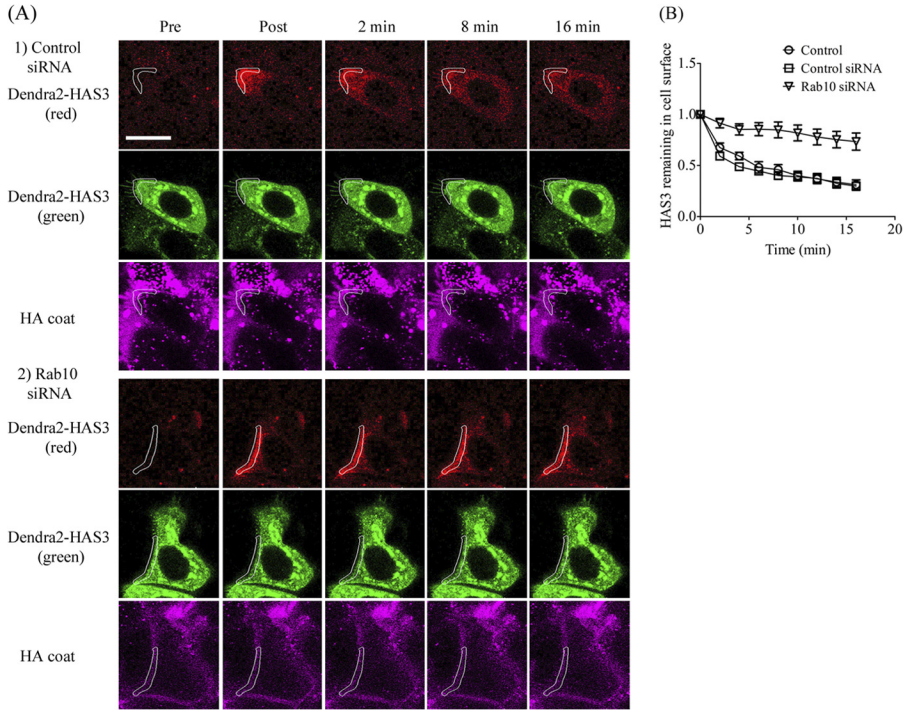

FIGURE 6. **Retrograde traffic of Dendra2-HAS3 from cell surface is decreased by Rab10 silencing.** *A*, siRNA-treated MCF7 cells were transfected with Dendra2-HAS3. The ROI was set to the cell surface using the inner edge of the HA coat, visualized by fHABC, as a marker. The selected region (*white line*) was photoconverted with 15% of the 405-nm laser power for 1 s. In control siRNA cells (*top set* of *panels*), the photoconverted Dendra2-HAS3 (*red channel*) from the cell surface was seen inside the cytoplasm already in 2–6 min, whereas the retrograde traffic of Dendra2-HAS3 (*red channel*) was slow following Rab10 silencing (*bottom set* of *panels*), even after 16 min. *Scale bar*, 20 μm. *B*, the kinetics of the Dendra2-HAS3 photoconverted to red in the cell surface was measured for a time span of 16 min at 2-min intervals. Rab10 silencing decreased the traffic of HAS3 from the cell surface to other parts of the cell. In the Rab10 silencing group at 16 min, on the average, 73% of the photoconverted Dendra2-HAS3 was left in the cell surface, whereas only 31 and 30% of the photoconverted Dendra2-HAS3 remained there in the control and control siRNA groups, respectively. Data represent the mean ± S.E. (*error bars*) of 3–5 independent experiments with 10 images per treatment and experiment. **, $p < 0.01$; ***, $p < 0.001$ for control *versus* Rab10 siRNA and control siRNA *versus* Rab10 siRNA, respectively (one-way ANOVA, Tukey's test).

the finding that Rab10 regulates the plasma membrane residence of HAS3 by endocytosis of HAS3, involving the clathrin-dependent pathway.

Rab10 Regulates Early Endocytosis of HAS3—To track the endocytosis pathway of HAS3 regulated by Rab10, we analyzed the colocalization of HAS3 with an early endocytosis marker, EEA1. Following Rab10 silencing, the cells were transiently transfected with EGFP-HAS3 and stained for EEA1. The EGFP-HAS3 strongly colocalized with EEA1 in the control and control siRNA groups, whereas in Rab10 silencing, the cells showed relatively less colocalization of EGFP-HAS3 and EEA1 (Fig. 9*A*). The image analysis was done in such a way that three ROIs were drawn at random sites outside of the nucleus and perinuclear Golgi region, and the average colocalization value was calculated from the ROIs. Quantitative analysis showed that Rab10 silencing indeed reduced the colocalization of EGFP-HAS3 with EEA1 to almost half ($Rr = 0.21$) compared with control siRNA ($Rr = 0.37$) and control ($Rr = 0.35$) groups (Fig. 9*B*). The data correlated well with the observation of reduced transferrin colocalization with HAS3 due to Rab10 silencing and further confirmed that Rab10 involvement in HAS3 trafficking takes place between plasma membrane and early endosomes.

Rab10 Silencing Decreases Cell Adhesion in an HA-dependent Manner—We then examined the consequences of Rab10 regulation of early endocytosis of HAS3 in a cell biological perspective. When making the MCF7-EGFP-HAS3 cells, we found that induction of HA synthesis by doxycycline reduced the increase of cell numbers during the following days in culture, in a dose-dependent manner (Fig. 10*A*). This prompted us to evaluate whether increased HA synthesis (coat formation and secretion) due to Rab10 silencing has a similar effect on the cell numbers. For this purpose, we used MCF7-EGFP-HAS3 cells induced to synthesize EGFP-HAS3 with 0.25 mg/ml doxycycline and parental MCF7 cells without HAS3 overexpression. The results showed that Rab10 silencing decreases cell numbers both in MCF7-EGFP-HAS3 (Fig. 10*B*) and parental MCF7 cells (Fig. 10*C*). Previous reports have shown that increased HA levels can result in reduced cell proliferation and adhesion (28). Interestingly, both HAS3 overexpression (14) and Rab10 knockdown (29) have shown disturbed epithelial polarization in MDCK cells, suggesting a defect in cell adhesion. This intrigued us, and we analyzed cell adhesion following Rab10 silencing to see if HAS3-induced HA synthesis disturbs this process. The results showed that Rab10 silencing decreased cell adhesion to collagen I to almost half, both in MCF7-EGFP-HAS3 (Fig. 10*D*) and parental MCF7 cells (Fig. 10*E*). We used hyaluronidase (5 transduction units/ml for 6 h) to remove the HA coat and signaling associated with it to see if the cell adhesion defect caused by Rab10 silencing is recovered. As expected, cell adhesion was partly rescued with hyaluronidase treatment in MCF7-EGFP-HAS3 cells, both in Rab10 and control siRNA

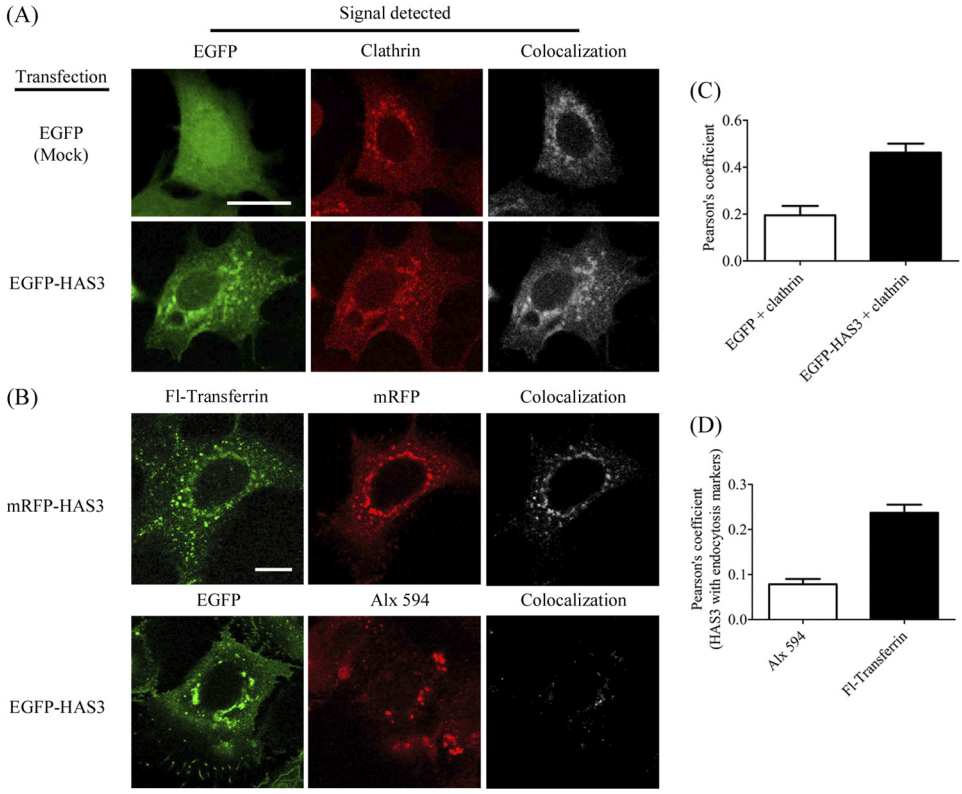

FIGURE 7. **HAS3 follows clathrin-dependent endocytosis.** *A*, EGFP-HAS3 showed a stronger colocalization with clathrin heavy chain (stained with anti-clathrin heavy chain antibody) in MCF7 cells, compared with mock transfection (EGFP). *Scale bar*, 25 μm. *B*, mRFP-HAS3 was also colocalized with fluorescein-transferrin, a marker for clathrin-dependent endocytosis, but not with Alexa Fluor® hydrazide 594 (*Alx 594*), a macropinocytosis marker. *Scale bar*, 10 μm. *C*, Pearson's correlation coefficient between clathrin heavy chain and EGFP-HAS3 ($Rr = 0.46$) was higher than EGFP only ($Rr = 0.19$). *D*, Pearson's correlation coefficient between mRFP-HAS3 and fluorescein-transferrin ($Rr = 0.23$) was significantly higher than EGFP-HAS3 and Alexa Fluor® hydrazide 594 ($Rr = 0.07$). Data in *C* and *D* represent mean ± S.E. (*error bars*) from three independent experiments with 10 images/group.

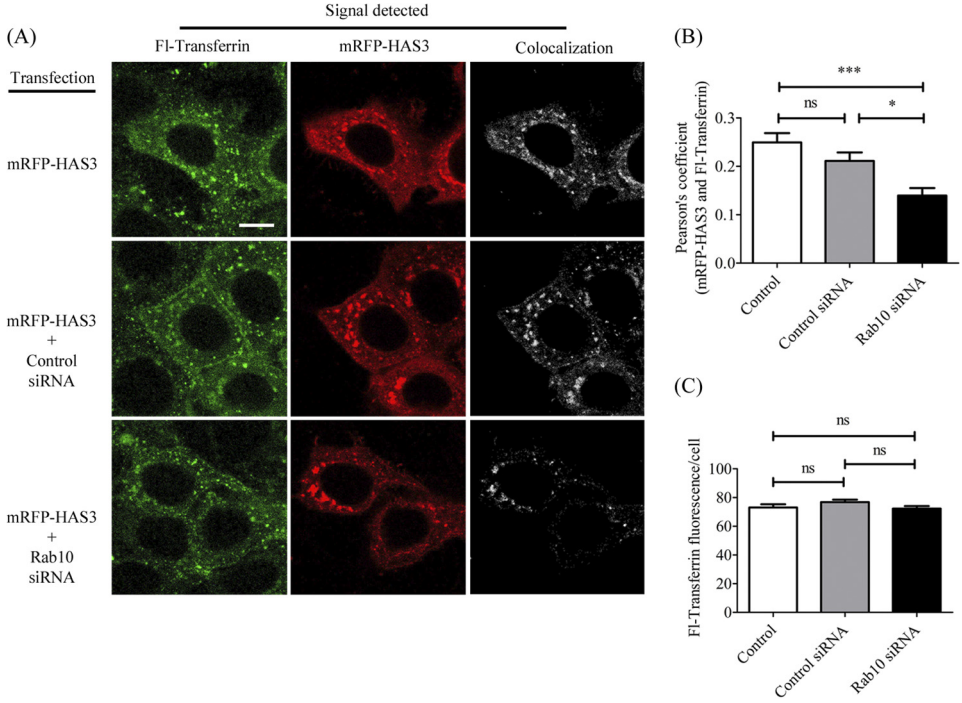

FIGURE 8. **Rab10 regulates clathrin-dependent endocytosis of HAS3.** *A*, siRNA-treated MCF7 cells were transfected with mRFP-HAS3, incubated with fluorescein-conjugated transferrin, and fixed with 4% PFA. Reduced colocalization between mRFP-HAS3 and fluorescein-transferrin was found following Rab10 silencing. *B*, Rab10 silencing significantly reduced the colocalization of mRFP-HAS3 with transferrin, compared with the control and control siRNA groups. *C*, the transferrin uptake, as measured by mean fluorescence intensity of the images, was not altered in the siRNA-treated groups. Data represent means ± S.E. (*error bars*) of three independent experiments with 15 images/group, taken with a ×63 oil objective. *, $p < 0.05$; ***, $p < 0.0001$; *ns*, not significant (one-way ANOVA, Tukey's test). *Scale bar*, 10 μm.

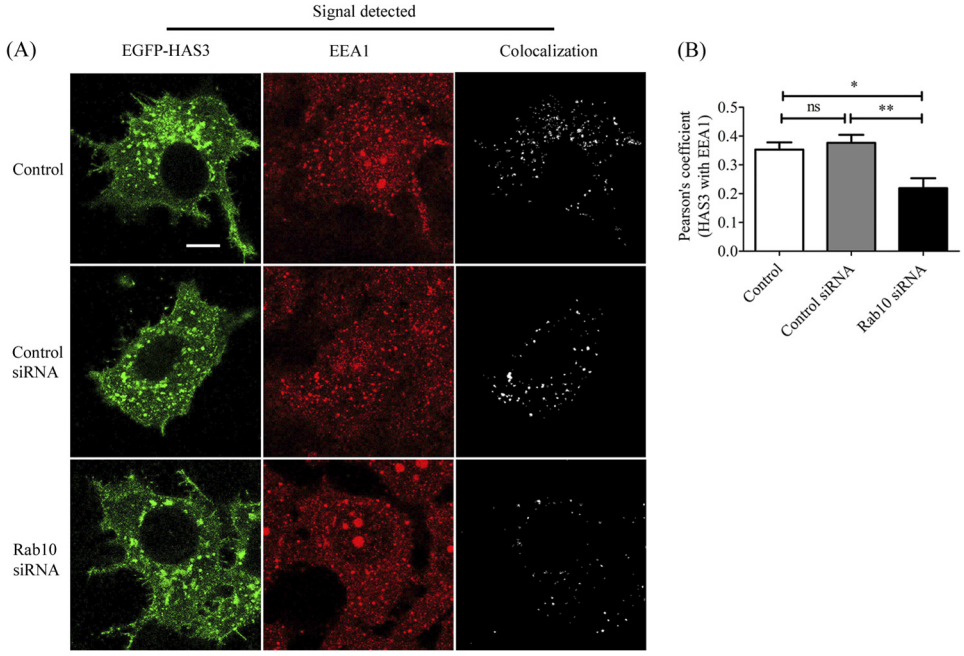

FIGURE 9. **Rab10 silencing decreases early endocytosis of HAS3.** *A*, siRNA-treated MCF7 cells were transfected with EGFP-HAS3, fixed, and stained for EEA1, an early endosomal marker. In the Rab10 silencing group, there were fewer EGFP-HAS3-positive vesicular structures, except in the Golgi area, and relatively less colocalization of EGFP-HAS3 and EEA1, compared with the control and control siRNA groups. *B*, quantitative analysis showed that EGFP-HAS3 colocalization with EEA1 was significantly reduced in Rab10 silencing, compared with control groups. Data represent means ± S.E. (*error bars*) of three independent experiments with 15 images/group, taken with a 63× oil objective. *, $p < 0.05$; **, $p < 0.005$; *ns*, not significant (one-way ANOVA, Tukey's test). The *colocalized panels* are shown as 1-bit images. *Scale bar*, 10 μm.

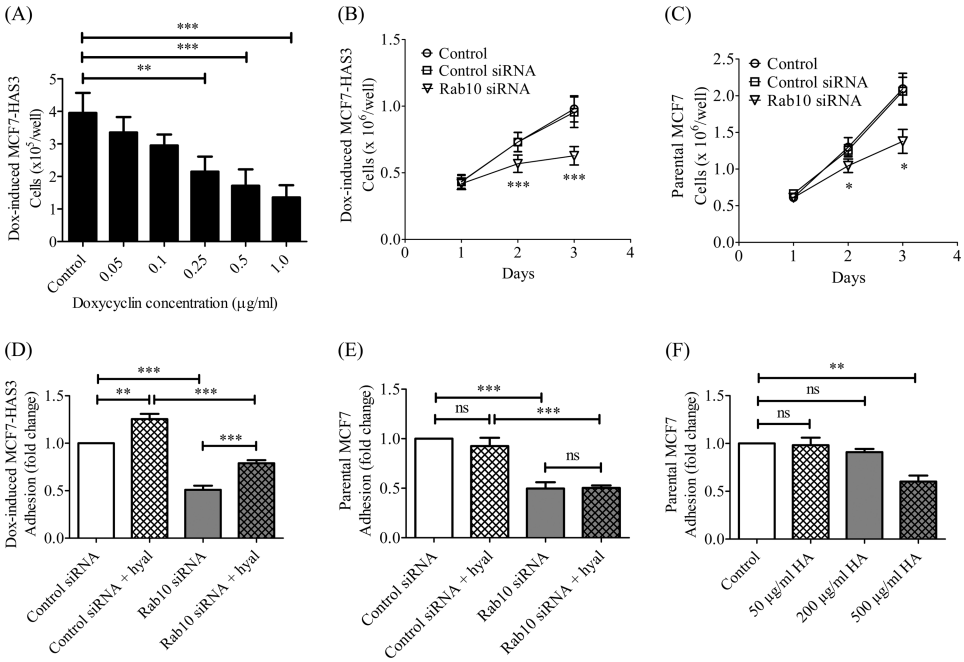

FIGURE 10. **HA-dependent reduction of cell adhesion with Rab10 silencing.** *A*, MCF7-EGFP-HAS3 cells with doxycycline-inducible EGFP-HAS3 expression showed a dose-dependent reduction of cell numbers after 48 h. Data represent means ± S.E. (*error bars*) of three independent experiments. *B*, Rab10 silencing decreased cell numbers in MCF7-EGFP-HAS3 cells induced to synthesize HA with 0.25 μg/ml doxycycline. *C*, Rab10 siRNA also reduced cell numbers in parental MCF7 cells. The data represent means ± S.E. of five and four independent experiments in *B* and *C*, respectively. *D*, 48 h post-transfection, Rab10 siRNA inhibits the adhesion of MCF7-EGFP-HAS3 cells, induced with 0.25 μg/ml doxycycline, whereas 5 transduction units/ml hyaluronidase for 6 h counteracts this by removing the HA coat, both in the cells with doxycycline-induced HA synthesis (*Control siRNA*) and those where HA synthesis was further enhanced by Rab10 siRNA. *E*, in a similar fashion, the MCF7 parental cells without enhanced HA synthesis were treated with Rab10 siRNA for 48 h and with 5 transduction units/ml of hyaluronidase for 6 h. There was a significant decrease in cell adhesion with Rab10 silencing but no effect by hyaluronidase in control or Rab10 siRNA groups. *F*, MCF7 parental cells were treated with exogenous, soluble HA, and cell adhesion to collagen I was analyzed as above. There was no significant decrease in adhesion, except in the cells treated with 500 μg/ml HA. The data represent means ± S.E. of three independent experiments in *D*, *E*, and *F*. *, $p < 0.05$; **, $p < 0.01$; ***, $p < 0.001$; *ns*, not significant (one-way ANOVA, Tukey's test).

groups (Fig. 10*D*) but not in MCF7 cells (Fig. 10*E*). The latter result is expected because in MCF7 cells, without HAS3 overexpression, there is negligible HA coat.

We then studied whether the adhesion block associated with HA synthesis was due to the HA secreted in the medium or rather the HA in the cell surface coat. Parental MCF7 cells produced ~0.13 μg/ml HA in the growth medium, which increased to ~6.2 μg/ml in MCF7-EGFP-HAS3 cells following induction with 0.25 μg/ml doxycycline. When we added purified, high molecular mass HA in the medium, concentrations up to 200 μg/ml showed no effect on cell adhesion to collagen I (Fig. 10*F*). With 500 μg/ml, the cell suspension became visibly viscous, obviously retarding the settling of the cells. Because an ~80-fold higher concentration of soluble HA was required to inhibit cell adhesion, the concentrations reached in the medium by endogenous or induced HA synthesis could not explain the reduced adhesion. We thus conclude that it is the HAS3-induced HA coat and/or its associated signaling to cell surface receptors that contributed to the reduced cell adhesion and that Rab10 silencing increased this effect.

DISCUSSION

We have identified Rab10 as the first known component in the specific trafficking machinery responsible for the control of HAS3 level in plasma membrane. It acts by increasing early endocytosis of HAS3 and results in changes in cell surface HA coat and HA secretion. As a consequence, Rab10 knockdown decreases cell adhesion of MCF7-EGFP-HAS3 cells to collagen in a HA-dependent mechanism and probably also influences a number of other HA-dependent cell functions.

Rab10 and Membrane Traffic—Rab GTPases are master regulators of intracellular traffic of proteins, lipids, and sometimes the whole organelles like Golgi and mitochondria (12, 30). Rab10 acts as a multifunctional regulator of intracellular traffic, including secretion of proteins and cargos from the *trans*-Golgi network and recycling endosomes to plasma membrane (12, 13, 31–34). Rab10 is also a well known regulator of exocytosis in many cell types (29, 35–37), as when it targets TGFα-containing exocytic vesicles to basolateral compartment in MDCK cells (38). Rab10 is a critical regulator of basement membrane secretion to the basal surface of *Drosophila* egg follicle cells (39) and promote the formation of new plasma membrane, maintaining axonal development and neuronal polarization (36). In addition, Rab10 has been shown to regulate the formation and dynamics of ER tubules (40), an effect that was not found in these cells subjected to a ~70% decline in Rab10 protein and using calnexin as a marker. Rab10 is also involved in the maturation of phagosomes in macrophages, perhaps by regulating the recycling of the components required for their maturation (41). Together with myosin-Va, Rab10 mediates the final steps in GLUT4-containing vesicle translocation to the plasma membrane (31).

Thus, most of the studies on Rab10 have demonstrated its role in forward trafficking of cargos from Golgi to plasma membrane and in recycling from endosomal compartments to plasma membrane. Indeed, none of the studies available has suggested that Rab10 can stimulate retrograde transport. The present study shows the unexpected stimulation by Rab10 of a specific cargo (HAS3) transport away from the plasma membrane. Whether Rab10 contributes directly to the initiation of HAS3 endocytosis or mediates the retraction of HAS3 from the plasma membrane with an indirect mechanism remains to be elucidated.

Polysaccharide Synthesis in Plasma Membrane—Chitin synthase and cellulose synthase are two glycosyltransferases similar to HAS in that they synthesize polysaccharides on the cell surface. The transport of chitin synthase appears to be completely different from that of HAS, which, unlike chitin synthase, is not dependent on microtubules but is sensitive to Brefeldin A (6, 7, 42). In *Drosophila*, the Rab protein Ypt32p stimulates the forward trafficking of endosomal chitin synthase Chs3p to the cell surface, resulting in enhanced chitin synthesis (43), whereas proteins involved in retrograde transport are not known. Endosomal targeting of yeast chitin synthase 3 (Chs3p) is associated with AP-1 and AP-3 complexes (44). The intracellular traffic of plant cellulose synthase, including its internalization from plasma membrane, is dependent both on actin and microtubule cytoskeletal elements and perhaps involves clathrin-dependent endocytosis (45). Thus, although information on the trafficking of the polysaccharide synthases active in the cell surface is still fragmentary, the other transferases in this group are probably transported by mechanisms quite different from vertebrate HAS.

HAS Trafficking as a Regulator of HA Synthesis—Numerous cytokines and growth factors like IL-1β, TNFα, and TGFβ are known to regulate the mRNA levels of different HASs (2), but the possible contribution of post-translational regulation has been difficult to discern. The present data show that a change in the trafficking machinery involving Rab10 can significantly modify the synthesis and cell surface presentation of HA. This finding raises the possibility that HAS trafficking is more important in the post-translational control of HA synthesis than previously thought. It is even possible that the previously described post-translational changes of HAS, like dimerization, monoubiquitination (10), and *O*-GlcNAc modification (11), influence HA synthesis through their effects on HAS trafficking. Indirect support for this idea is offered by findings indicating that virtually all Golgi glycosyltransferases form homo- and heteromers, which influences their trafficking between Golgi and ER (46). Ubiquitination is also associated with protein transfer between certain cell compartments (47). Furthermore, *O*-GlcNAcylation of HAS2 increases its stability (half-life) (11), which is compatible with the hypothesis that the *O*-GlcNAc moiety acts as a signal that reduces HAS traffic to catabolic compartments. Indeed, sufficient cellular UDP-GlcNAc content is required for HASs to stay in the plasma membrane (16). We can thus speculate that a high concentration of UDP-GlcNAc increases the *O*-GlcNAc level of HAS2, which serves as a signal that contributes to its presence in the plasma membrane by preventing exit into catabolic pathways. Future studies must explore the possible association between the trafficking of HASs and their post-translational covalent modifications.

Half-life of HAS3 in Plasma Membrane—The short (~5–6-min) average half-life of Dendra2-HAS3 in plasma membrane was unexpected, given the ~2 h required to clear keratinocyte

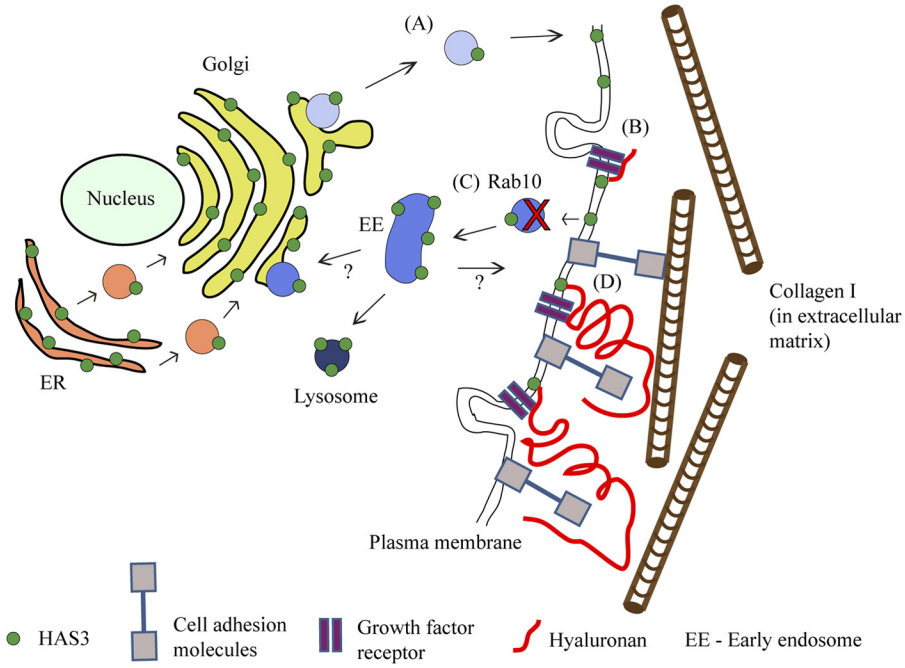

FIGURE 11. **Scheme suggesting the traffic of HAS3 and the role of Rab10 in HA synthesis and cell adhesion.** *A*, HAS3-containing transport vesicles have a constant flux between plasma membrane and cytoplasm with an average $t_{1/2}$ of ~5–6 min. *B*, however, HAS3 with an ongoing HA synthesis remains stable in the membrane with a $t_{1/2}$ of 2–4 h. *C*, Rab10 enhances the early endocytosis of HAS3. When Rab10 is knocked down (*red cross*), the average time that HAS3 spends in the plasma membrane is increased, enhancing the probability of HA synthesis initiation. *D*, the HA coat enlarged by Rab10 knockdown counteracts the effect of cell surface adhesion molecules, resulting in impaired cell adhesion to collagen I.

plasma membrane from EGFP-HAS3 following introduction of Brefeldin A to block the entry of new EGFP-HAS3 from Golgi (7). Studies on HAS in fibroblasts (48) and *Xenopus* cells (49) also suggest that the time required to synthesize a single, full-length (>1-MDa) HA chain takes up to ~3–4 h. These findings can be reconciled by assuming that the endocytosis we detect excludes those HAS3s that have started HA chain synthesis. Then, while there is a constant flux of HAS3 vesicles to the plasma membrane and an equally fast return into the cytoplasm, those HASs that have succeeded in starting HA synthesis remain in the plasma membrane. Retardation of the reverse traffic by blocking Rab10 should then increase the average dwell time of HAS3 in the plasma membrane, enhancing its chance of starting HA synthesis (Fig. 11). This stochastic model of initiation of HA synthesis by HAS3 also accommodates the fact that the concentration of substrates (UDP-GlcUA and UDP-GlcNAc) contributes to the abundance of HAS in the plasma membrane (16). Moreover, if similar trafficking and chain initiation takes place with other HASs, it explains why HAS1 (the member of the HAS family with the highest K_m values for the substrates) is seldom present in the plasma membrane, whereas HAS3 (with the lowest K_m values) is most abundant there (16).

Rab10-mediated Control of HA Synthesis, Cell Adhesion, and Possible Consequences in Malignant Growth—Enhanced HA synthesis driven by HAS3 causes mitotic spindle misorientation and epithelial structure disruption that may facilitate carcinogenesis (14). HAS3 was recently found to dramatically increase shedding of extracellular microvesicles (50) that have also been associated with cancer spreading and metastasis (51). Indeed, overexpression of HAS3 has often been reported in cancers (52–54), and suppression of HAS3 expression leads to apoptosis and inhibition of tumor growth (55, 56).

Interestingly, just like HAS3 overexpression (14), Rab10 knockdown results in disturbed epithelial polarization (29). The present data thus raise the possibility that the HA coat on the cell surface may sterically or by currently unknown signaling systems retard intercellular adhesion in the same way as it reduced binding to collagen and thus disturb the normal architecture of epithelium. Rab10 suppression of HAS3-dependent HA synthesis may represent an important checkpoint for malignant growth. In the future, the connection of this Rab10- and HA-mediated control of cell adhesion with the development of epithelial-to-mesenchymal transition, invasion, and metastasis of cancer cells will be explored.

Acknowledgments—We thank Pasi Kankaanpää M.S. for expert guidance in image processing, Dr. Sanna Pasonen-Seppänen and Piia Takabe M.S. for consultation and technical assistance, Dr. Daniel Abankwa and Dr. Sakari Kellokumpu for critical evaluation of the project goals, Yashwanth Ashok M.S. for consultation, and Tuula Venäläinen for preparation of the fluorescent HABC.

REFERENCES

1. DeAngelis, P. L. (2002) Evolution of glycosaminoglycans and their glycosyltransferases: Implications for the extracellular matrices of animals and the capsules of pathogenic bacteria. *Anat. Rec.* **268,** 317–326
2. Jiang, D., Liang, J., and Noble, P. W. (2011) Hyaluronan as an immune regulator in human diseases. *Physiol. Rev.* **91,** 221–264
3. Sironen, R. K., Tammi, M., Tammi, R., Auvinen, P. K., Anttila, M., and Kosma, V. M. (2011) Hyaluronan in human malignancies. *Exp. Cell Res.* **317,** 383–391
4. Toole, B. P. (2004) Hyaluronan: from extracellular glue to pericellular cue.

Nat. Rev. Cancer. **4,** 528–539
5. Weigel, P. H., and DeAngelis, P. L. (2007) Hyaluronan synthases: a decade-plus of novel glycosyltransferases. *J. Biol. Chem.* **282,** 36777–36781
6. Kultti, A., Rilla, K., Tiihonen, R., Spicer, A. P., Tammi, R. H., and Tammi, M. I. (2006) Hyaluronan synthesis induces microvillus-like cell surface protrusions. *J. Biol. Chem.* **281,** 15821–15828
7. Rilla, K., Siiskonen, H., Spicer, A. P., Hyttinen, J. M., Tammi, M. I., and Tammi, R. H. (2005) Plasma membrane residence of hyaluronan synthase is coupled to its enzymatic activity. *J. Biol. Chem.* **280,** 31890–31897
8. Tammi, R. H., Passi, A. G., Rilla, K., Karousou, E., Vigetti, D., Makkonen, K., and Tammi, M. I. (2011) Transcriptional and post-translational regulation of hyaluronan synthesis. *FEBS J.* **278,** 1419–1428
9. Goentzel, B. J., Weigel, P. H., and Steinberg, R. A. (2006) Recombinant human hyaluronan synthase 3 is phosphorylated in mammalian cells. *Biochem. J.* **396,** 347–354
10. Karousou, E., Kamiryo, M., Skandalis, S. S., Ruusala, A., Asteriou, T., Passi, A., Yamashita, H., Hellman, U., Heldin, C. H., and Heldin, P. (2010) The activity of hyaluronan synthase 2 is regulated by dimerization and ubiquitination. *J. Biol. Chem.* **285,** 23647–23654
11. Vigetti, D., Deleonibus, S., Moretto, P., Karousou, E., Viola, M., Bartolini, B., Hascall, V. C., Tammi, M., De Luca, G., and Passi, A. (2012) Role of UDP-*N*-acetylglucosamine (GlcNAc) and *O*-GlcNAcylation of hyaluronan synthase 2 in the control of chondroitin sulfate and hyaluronan synthesis. *J. Biol. Chem.* **287,** 35544–35555
12. Hutagalung, A. H., and Novick, P. J. (2011) Role of Rab GTPases in membrane traffic and cell physiology. *Physiol. Rev.* **91,** 119–149
13. Schwartz, S. L., Cao, C., Pylypenko, O., Rak, A., and Wandinger-Ness, A. (2007) Rab GTPases at a glance. *J. Cell Sci.* **120,** 3905–3910
14. Rilla, K., Pasonen-Seppänen, S., Kärnä, R., Karjalainen, H. M., Törrönen, K., Koistinen, V., Tammi, M. I., Tammi, R. H., Teräväinen, T., and Manninen, A. (2012) HAS3-induced accumulation of hyaluronan in 3D MDCK cultures results in mitotic spindle misorientation and disturbed organization of epithelium. *Histochem. Cell Biol.* **137,** 153–164
15. Siiskonen, H., Rilla, K., Kärnä, R., Bart, G., Jing, W., Haller, M. F., DeAngelis, P. L., Tammi, R. H., and Tammi, M. I. (2013) Hyaluronan in cytosol-microinjection-based probing of its existence and suggested functions. *Glycobiology* **23,** 222–231
16. Rilla, K., Oikari, S., Jokela, T. A., Hyttinen, J. M., Kärnä, R., Tammi, R. H., and Tammi, M. I. (2013) Hyaluronan synthase 1 (HAS1) requires higher cellular UDP-GlcNAc concentration than HAS2 and HAS3. *J. Biol. Chem.* **288,** 5973–5983
17. Yeung, T., Terebiznik, M., Yu, L., Silvius, J., Abidi, W. M., Philips, M., Levine, T., Kapus, A., and Grinstein, S. (2006) Receptor activation alters inner surface potential during phagocytosis. *Science* **313,** 347–351
18. Hassinen, A., Pujol, F. M., Kokkonen, N., Pieters, C., Kihlström, M., Korhonen, K., and Kellokumpu, S. (2011) Functional organization of Golgi *N*- and *O*-glycosylation pathways involves pH-dependent complex formation that is impaired in cancer cells. *J. Biol. Chem.* **286,** 38329–38340
19. Piltti, J., Häyrinen, J., Karjalainen, H. M., and Lammi, M. J. (2008) Proteomics of chondrocytes with special reference to phosphorylation changes of proteins in stretched human chondrosarcoma cells. *Biorheology* **45,** 323–335
20. Yates, J. R., 3rd, Eng, J. K., and McCormack, A. L. (1995) Mining genomes: correlating tandem mass spectra of modified and unmodified peptides to sequences in nucleotide databases. *Anal. Chem.* **67,** 3202–3210
21. Perkins, D. N., Pappin, D. J., Creasy, D. M., and Cottrell, J. S. (1999) Probability-based protein identification by searching sequence databases using mass spectrometry data. *Electrophoresis* **20,** 3551–3567
22. Hiltunen, E. L., Anttila, M., Kultti, A., Ropponen, K., Penttinen, J., Yliskoski, M., Kuronen, A. T., Juhola, M., Tammi, R., Tammi, M., and Kosma, V. M. (2002) Elevated hyaluronan concentration without hyaluronidase activation in malignant epithelial ovarian tumors. *Cancer Res.* **62,** 6410–6413
23. Kankaanpää, P., Paavolainen, L., Tiitta, S., Karjalainen, M., Päivärinne, J., Nieminen, J., Marjomäki, V., Heino, J., and White, D. J. (2012) BioImageXD: an open, general-purpose and high-throughput image-processing platform. *Nat. Methods* **9,** 683–689
24. Bastiaens, P. I., Majoul, I. V., Verveer, P. J., Söling, H. D., and Jovin, T. M. (1996) Imaging the intracellular trafficking and state of the AB5 quaternary structure of cholera toxin. *EMBO J.* **15,** 4246–4253
25. Rilla, K., Tiihonen, R., Kultti, A., Tammi, M., and Tammi, R. (2008) Pericellular hyaluronan coat visualized in live cells with a fluorescent probe is scaffolded by plasma membrane protrusions. *J. Histochem. Cytochem.* **56,** 901–910
26. Boucrot, E., Saffarian, S., Zhang, R., and Kirchhausen, T. (2010) Roles of AP-2 in clathrin-mediated endocytosis. *PLoS One* **5,** e10597
27. Doyon, J. B., Zeitler, B., Cheng, J., Cheng, A. T., Cherone, J. M., Santiago, Y., Lee, A. H., Vo, T. D., Doyon, Y., Miller, J. C., Paschon, D. E., Zhang, L., Rebar, E. J., Gregory, P. D., Urnov, F. D., and Drubin, D. G. (2011) Rapid and efficient clathrin-mediated endocytosis revealed in genome-edited mammalian cells. *Nat. Cell Biol.* **13,** 331–337
28. Dübe, B., Lüke, H. J., Aumailley, M., and Prehm, P. (2001) Hyaluronan reduces migration and proliferation in CHO cells. *Biochim. Biophys. Acta* **1538,** 283–289
29. Schuck, S., Gerl, M. J., Ang, A., Manninen, A., Keller, P., Mellman, I., and Simons, K. (2007) Rab10 is involved in basolateral transport in polarized Madin-Darby canine kidney cells. *Traffic* **8,** 47–60
30. Stenmark, H. (2009) Rab GTPases as coordinators of vesicle traffic. *Nat. Rev. Mol. Cell Biol.* **10,** 513–525
31. Chen, Y., Wang, Y., Zhang, J., Deng, Y., Jiang, L., Song, E., Wu, X. S., Hammer, J. A., Xu, T., and Lippincott-Schwartz, J. (2012) Rab10 and myosin-Va mediate insulin-stimulated GLUT4 storage vesicle translocation in adipocytes. *J. Cell Biol.* **198,** 545–560
32. Shi, A., Liu, O., Koenig, S., Banerjee, R., Chen, C. C., Eimer, S., and Grant, B. D. (2012) RAB-10-GTPase-mediated regulation of endosomal phosphatidylinositol-4,5-bisphosphate. *Proc. Natl. Acad. Sci. U.S.A.* **109,** E2306–E2315
33. Wang, D., Lou, J., Ouyang, C., Chen, W., Liu, Y., Liu, X., Cao, X., Wang, J., and Lu, L. (2010) Ras-related protein Rab10 facilitates TLR4 signaling by promoting replenishment of TLR4 onto the plasma membrane. *Proc. Natl. Acad. Sci. U.S.A.* **107,** 13806–13811
34. Babbey, C. M., Ahktar, N., Wang, E., Chen, C. C., Grant, B. D., and Dunn, K. W. (2006) Rab10 regulates membrane transport through early endosomes of polarized Madin-Darby canine kidney cells. *Mol. Biol. Cell* **17,** 3156–3175
35. Sano, H., Eguez, L., Teruel, M. N., Fukuda, M., Chuang, T. D., Chavez, J. A., Lienhard, G. E., and McGraw, T. E. (2007) Rab10, a target of the AS160 Rab GAP, is required for insulin-stimulated translocation of GLUT4 to the adipocyte plasma membrane. *Cell Metab.* **5,** 293–303
36. Wang, T., Liu, Y., Xu, X. H., Deng, C. Y., Wu, K. Y., Zhu, J., Fu, X. Q., He, M., and Luo, Z. G. (2011) Lgl1 activation of rab10 promotes axonal membrane trafficking underlying neuronal polarization. *Dev. Cell* **21,** 431–444
37. Babbey, C. M., Bacallao, R. L., and Dunn, K. W. (2010) Rab10 associates with primary cilia and the exocyst complex in renal epithelial cells. *Am. J. Physiol. Renal Physiol.* **299,** F495–F506
38. Cao, Z., Li, C., Higginbotham, J. N., Franklin, J. L., Tabb, D. L., Graves-Deal, R., Hill, S., Cheek, K., Jerome, W. G., Lapierre, L. A., Goldenring, J. R., Ham, A. J., and Coffey, R. J. (2008) Use of fluorescence-activated vesicle sorting for isolation of Naked2-associated, basolaterally targeted exocytic vesicles for proteomics analysis. *Mol. Cell Proteomics* **7,** 1651–1667
39. Lerner, D. W., McCoy, D., Isabella, A. J., Mahowald, A. P., Gerlach, G. F., Chaudhry, T. A., and Horne-Badovinac, S. (2013) A Rab10-dependent mechanism for polarized basement membrane secretion during organ morphogenesis. *Dev. Cell* **24,** 159–168
40. English, A. R., and Voeltz, G. K. (2013) Rab10 GTPase regulates ER dynamics and morphology. *Nat. Cell Biol.* **15,** 169–178
41. Cardoso, C. M., Jordao, L., and Vieira, O. V. (2010) Rab10 regulates phagosome maturation and its overexpression rescues Mycobacterium-containing phagosomes maturation. *Traffic* **11,** 221–235
42. Sánchez-León, E., Verdín, J., Freitag, M., Roberson, R. W., Bartnicki-Garcia, S., and Riquelme, M. (2011) Traffic of chitin synthase 1 (CHS-1) to the Spitzenkorper and developing septa in hyphae of *Neurospora crassa*: actin dependence and evidence of distinct microvesicle populations. *Eukaryot. Cell.* **10,** 683–695
43. Ortiz, D., and Novick, P. J. (2006) Ypt32p regulates the translocation of Chs3p from an internal pool to the plasma membrane. *Eur. J. Cell Biol.* **85,**

107–116
44. Starr, T. L., Pagant, S., Wang, C. W., and Schekman, R. (2012) Sorting signals that mediate traffic of chitin synthase III between the TGN/endosomes and to the plasma membrane in yeast. *PLoS One* **7,** e46386
45. Crowell, E. F., Gonneau, M., Stierhof, Y. D., Höfte, H., and Vernhettes, S. (2010) Regulated trafficking of cellulose synthases. *Curr. Opin. Plant Biol.* **13,** 700–705
46. Hassinen, A., Rivinoja, A., Kauppila, A., and Kellokumpu, S. (2010) Golgi *N*-glycosyltransferases form both homo- and heterodimeric enzyme complexes in live cells. *J. Biol. Chem.* **285,** 17771–17777
47. Tanno, H., and Komada, M. (2013) The ubiquitin code and its decoding machinery in the endocytic pathway. *J. Biochem.* **153,** 497–504
48. Kitchen, J. R., and Cysyk, R. L. (1995) Synthesis and release of hyaluronic acid by Swiss 3T3 fibroblasts. *Biochem. J.* **309,** 649–656
49. Pummill, P. E., Achyuthan, A. M., and DeAngelis, P. L. (1998) Enzymological characterization of recombinant xenopus DG42, a vertebrate hyaluronan synthase. *J. Biol. Chem.* **273,** 4976–4981
50. Rilla, K., Pasonen-Seppänen, S., Deen, A. J., Koistinen, V. V., Wojciechowski, S., Oikari, S., Kärnä, R., Bart, G., Törrönen, K., Tammi, R. H., and Tammi, M. I. (2013) Hyaluronan production enhances shedding of plasma membrane-derived microvesicles. *Exp. Cell Res.* **319,** 2006–2018
51. Muralidharan-Chari, V., Clancy, J. W., Sedgwick, A., and D'Souza-Schorey, C. (2010) Microvesicles: mediators of extracellular communication during cancer progression. *J. Cell Sci.* **123,** 1603–1611
52. Tzellos, T. G., Kyrgidis, A., Vahtsevanos, K., Triaridis, S., Printza, A., Klagas, I., Zvintzou, E., Kritis, A., Karakiulakis, G., and Papakonstantinou, E. (2011) Nodular basal cell carcinoma is associated with increased hyaluronan homeostasis. *J. Eur. Acad. Dermatol. Venereol.* **25,** 679–687
53. Kanomata, N., Yokose, T., Kamijo, T., Yonou, H., Hasebe, T., Itano, N., Kimata, K., and Ochiai, A. (2005) Hyaluronan synthase expression in pleural malignant mesotheliomas. *Virchows Arch.* **446,** 246–250
54. Nykopp, T. K., Rilla, K., Tammi, M. I., Tammi, R. H., Sironen, R., Hämäläinen, K., Kosma, V. M., Heinonen, S., and Anttila, M. (2010) Hyaluronan synthases (HAS1–3) and hyaluronidases (HYAL1–2) in the accumulation of hyaluronan in endometrioid endometrial carcinoma. *BMC Cancer* **10,** 512
55. Twarock, S., Freudenberger, T., Poscher, E., Dai, G., Jannasch, K., Dullin, C., Alves, F., Prenzel, K., Knoefel, W. T., Stoecklein, N. H., Savani, R. C., Homey, B., and Fischer, J. W. (2011) Inhibition of oesophageal squamous cell carcinoma progression by in vivo targeting of hyaluronan synthesis. *Mol. Cancer* **10,** 30
56. Teng, B. P., Heffler, M. D., Lai, E. C., Zhao, Y. L., LeVea, C. M., Golubovskaya, V. M., and Bullarddunn, K. M. (2011) Inhibition of hyaluronan synthase-3 decreases subcutaneous colon cancer growth by increasing apoptosis. *Anticancer Agents Med. Chem.* **11,** 620–628